INTEGRATING CARTILAGE-SPECIFIC T1RHO MRI INTO KNEE CLINIC DIAGNOSTIC IMAGING

Douglas R Pedersen, Ph.D.,* Noelle F Klocke, B.S.E.,* Daniel R Thedens, Ph.D.,**
James A Martin, Ph.D.,* Glenn N Williams, Ph.D.,*,† Annunziato Amendola, M.D.*

ABSTRACT

With a rise in post-traumatic osteoarthritis, OA no longer is considered just a disease of aging. The 'gold standard' for OA diagnosis has long been planar radiographs for visualizing osteophytes, joint space narrowing and sclerotic changes. A typical magnetic resonance imaging (MRI) protocol will acquire proton density, T1, T2, and fat suppressed images that give a comprehensive picture of morphologic changes associated with injury and subsequent degenerative processes. However, the earliest events of cartilage degeneration occur within the tissue, before measureable changes in morphology. MRI methods have been proposed to display and quantify changes in composition and integrity of such elements of cartilage extracellular matrix as collagen and proteoglycan (PG) content in vivo. T1ρ, the spin-lattice relaxation time in the rotating frame, has come to the forefront for visualizing water proton–PG interactions in articular cartilage.

The purpose of this T1ρ MRI study was to define an objective femoral condyle-specific registration method, in which zone-dependent cartilage compositional changes could be assessed from the bone outward through the existing cartilage, at pre-ACL reconstruction and subsequent follow-up times, when the loss of thickness to surface-down cartilage erosion might occur later in the OA pathogenesis. Additionally, this study explores the effects of reducing the number of spin-lock times on the absolute T1ρ relaxation times; a major parameter in expanding T1ρ coverage to the whole joint while satisfying clinical imaging time and specific absorption rate (SAR) safety constraints.

The developed image analysis tools serve as the first step toward quantitative functional assessment of cartilage health with noninvasive T1ρ MRI, which has the potential to become an important new tool for the early diagnosis of cartilage degeneration following ACL trauma.

INTRODUCTION

As recently as October, 2010, the CDC reported osteoarthritis as a growing public health problem that continues to be the most common cause of disability, at an annual cost of $128 billion.[1] With a rise in post-traumatic osteoarthritis (PTOA) OA no longer is considered just a disease of aging.[2] The 'gold standard' for OA diagnosis has long been planar radiographs for visualizing osteophytes, joint space narrowing and sclerotic changes. Exquisite soft-tissue definition from the multiplicity of contrast mechanisms available in a single exam have established magnetic resonance imaging (MRI) as the method of choice for visualization of cartilage and joint anatomy in a wide range of clinical applications. A typical MRI protocol will acquire proton density, T1, T2, and fat suppressed images, which give a comprehensive picture of morphologic changes associated with injury and subsequent degenerative processes.[3] Nevertheless, a lack of noninvasive quantitative measures of cartilage condition *in vivo* prevents meaningful assessment of joint injuries, thus making early treatment effects difficult to verify.

Multi-center studies such as the Osteoarthritis Initiative (OAI) target identifying chemical and imaging biomarkers for evaluating the progression and risk factors of symptomatic knee OA.[4] These studies stimulated development of 3-dimensional MRI to better quantify articular cartilage thickness changes earlier in the OA etiology, with several cartilage–bone–shape segmentation and analysis methods reported.[5-8] Knee zones nomenclature[9] and cartilage metrics (WORMS)[10] have been defined to establish common comparative measurements. Recent reports from these large cohort studies document changes in femorotibial cartilage thickness and extent of denuded areas of bone as they relate to the radiographic stages of OA.[11, 12]

*Department of Orthopaedics & Rehabilitation, University of Iowa, Iowa City, IA, USA

**Department of Radiology, University of Iowa, Iowa City, IA, USA

†Physical Therapy & Rehabilitation Science, University of Iowa, Iowa City, IA, USA

Corresponding Author:
Douglas R Pedersen
2181 Westlawn Building, Iowa City, IA 52242-1100
Telephone: 319-335-7533
Fax: 319-335-7530
Email: doug-pedersen@uiowa.edu

Grant Support: NIH NIAMS P50 AR055533 and AOSSM Research Grant

However, the earliest events of cartilage degeneration occur within the tissue, before measureable changes in morphology.[2, 13] Therefore, detection and treatment of PTOA joint degeneration occurs later in the process. MRI methods have been proposed to display and quantify changes in composition and integrity of such elements of cartilage extracellular matrix as collagen and proteoglycan (PG) content *in vivo*.[14-16] These cartilage-composition MRI sequences involve multiple time-step image captures and post processing of voxel-wise exponential fits to determine relaxivity time constants. In healthy cartilage, the collagen matrix restricts water molecule movement inducing an effective dipole-dipole interaction. This interaction depends on collagen fiber orientation within the external magnetic field; thereby making the T2 relaxation time sensitive to fiber orientation and water content in cartilage.[17-20] Magic-angle imaging, in which the angle dependence of T2 is measured, can provide a specific measure of collagen ultrastructure. However, the difficulty in getting the angle dependence presently precludes its use clinically. Despite the fact that T2 relaxation time imaging is available on most clinical MRI platforms, the variety of hardware-software implementations produces differing ranges of T2 values that confound direct study results comparisons.

Delayed gadolinium-enhanced MRI of cartilage (dGEMRIC) provides a specific measure of glycosaminoglycan (GAG) concentration.[21-23] This method measures the distribution of a charged contrast agent, which in turn reflects the distribution of charge associated with GAG, of which proteoglycan (PG) is the dominant component. The exogenous agent requires 90-120 minutes to permeate the extracellular cartilage matrix after intravenous injection. The two hour delay between the baseline and the diagnostic T1-inversion recovery sequence imaging sessions make this logistically difficult in the clinical setting. Additionally, gadopentetate contrast injection $Gd(DPTA)^{2-}$, has been associated with Nephrogenic Systemic Fibrosis or Nephrogenic Fibrosing Dermopathy (NSF/NFD), which renders the contrast agent unsuitable for patients with any glomerular filtration inadequacies.[24, 25]

T1ρ, the spin-lattice relaxation time in the rotating frame, has come to the forefront for visualizing water proton–PG interactions in articular cartilage.[26-28] Non-invasive cartilage-specific T1ρ provides a continuous measure of joint condition by utilizing a pre-encoded spin-lock pulse cluster followed by a fast spin echo (FSE) image capture. In the research setting these have also been acquired in 3-D, where the longer data acquisition times can be accommodated.[29] However, in the clinical setting, speed, resolution, joint coverage and signal-to-noise ratio (SNR) must be balanced with other diagnostic imaging demands as reported in a state-of-the-art review of imaging outcome measurement in OA.[30]

Prior to cartilage-specific sequences, MRI was used as a diagnostic tool for suspected acute internal derangement of the knee. In a controlled, prospective study of suspected ACL injuries, the common orthogonal (sagittal) MRI images were compared to non-orthogonal (oblique sagittal) imaging of the knee.[31] In all measures, 60-70% diagnosis success with standard orthogonal views jumped to 100% with the oblique sagittal views aligned to contain the mid-substance of the ACL. This orientation was maintained when we introduced T2, dGEMRIC and T1ρ in an on-going prospective clinical evaluation of cartilage-specific MRI sequences in acute ACL rupture patients. To keep the image sessions under an hour in length, selected 2-D oblique sagittal slices were acquired to provide compositional insight into immediate post-traumatic response in the load bearing lateral condyle cartilage where most of the initial injury occurs.

The purpose of this study was to define an objective condyle-specific registration method, in which zone-dependent cartilage compositional changes could be assessed from the bone outward through the existing cartilage, at pre-ACLR and subsequent follow-up times, when the loss of thickness to surface-down cartilage erosion might occur later in the OA pathogenesis. Additionally, this study explores the effects of reducing the number of spin-lock times on the absolute T1ρ relaxation times; a major parameter in expanding T1ρ coverage to the whole joint while satisfying time and specific absorption rate (SAR) safety constraints.

METHODS

In an on-going prospective clinical evaluation of cartilage-specific MRI, we have gathered T1ρ FSE (fast spin echo) images to assess the sensitivity of T1ρ measures of water-PG interactions *in vivo*. Diagnostic MRI images were obtained from seven healthy subjects with no history of knee injury or symptoms of osteoarthritis (Table 1). Three scanning sessions of one knee in each normal subject were performed at the same hour of alternate days to assess the consistency of image quality and fluctuations in day-to-day cartilage condition. Study protocol and informed consent documentation were approved by the Institutional Review Board.

Histology-based criterion for T1ρ cartilage sampling

An above-knee amputation (AKA) for a proximal femur sarcoma was imaged intact and then disarticulated for coronal and sagittal safranin-O histology to provide a cartilage composition frame of reference for cartilage-specific T1ρ MRI (Figure 1). The osteochondral speci-

TABLE 1
Normal Subjects' Demographics

Normal	Gender	Age	Knee
1	Male	59	Left
2	Female	23	Left
3	Male	22	Right
4	Female	22	Left
5	Male	59	Left
6	Male	23	Right
7	Female	23	Left

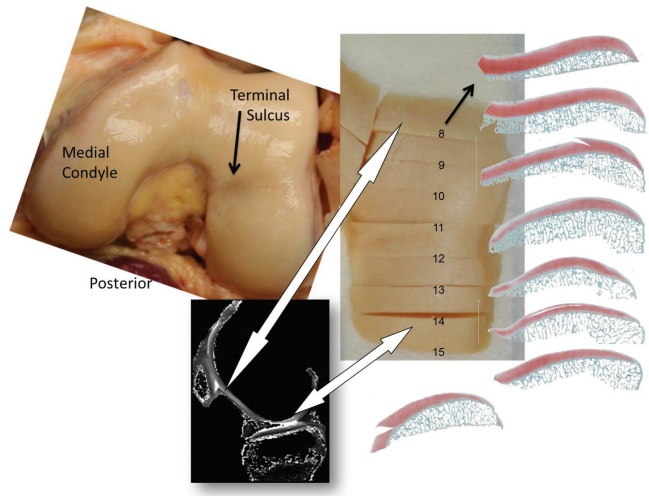

Figure 1. Photographs are of the AKA intact distal femur and of the lateral condyle after sectioning perpendicular to the condylar midline. Histology sections were obtained at each of the eight osteochondral blocks' posterior faces. The condyle is 20-25 mm wide.

mens were fixed, decalcified and embedded in paraffin. Multiple 5μm thick microtome slices were mounted serially for staining and image analysis similar to those utilized in cartilage repair scoring systems [32-35] with their origins in the Mankin cartilage OA grading system.[36, 37] The sections were stained with Weigert's hematoxylin, safranin-O, and fast green. Weigert's hematoxylin stains chondrocyte nuclei black to enhance digital identification of nuclear material. Safranin-O is a cationic dye that binds specifically and stoichiometrically to sulfated glycosaminoglycans, and the intensity of the red stain indicates proteoglycan (PG) content.[38] Fast Green provides a contrasting counter-stain. Each histology section samples a 5μm thick strip across the condyle weight-bearing width.

Patient imaging

MRI image plane alignment was determined by standard clinical practice for knee injury diagnosis. The oblique sagittal images were aligned to contain the midsubstance of the ACL in a single slice; not orthogonal patient-defined sagittal, coronal and axial images. Images were acquired on a 3T Siemens TIM Trio scanner (Siemens Medical Solutions, Erlangen, Germany) using a single channel transmit-receive extremity coil and a multi-slice T1ρ magnetization preparation step followed by a fast spin-echo image protocol (TR=3000 ms, TE=9.5 ms). The T1ρ magnetization preparation step consists of a +90°x tip-down, 400 Hz self-compensating spin-lock RF of variable duration (5, 10, 20, 40, 60, 80 ms) for T1ρ weighting, and a -90°x tip-up and final crusher gradient.[39] In-plane image resolution of 0.55 mm/voxel in a 140 x 140 mm field of view was acquired with slice thickness of 4 mm, and 8 mm spacing between slice centers. These oblique sagittal 0.5×0.5×4 mm^3 voxel slices sample the continuum of cartilage composition in the lateral condyle, in addition to current knee injury diagnostic MRI sequences (Table 2). The T1- and T2-weighted images are also used for assessing various masses, Baker's cyst, etc. as this is a very general purpose protocol.

Bone-cartilage interface (BCI) definition

Image analysis was developed in Matlab® (Mathworks, Inc., Natick, MA). A multi-directional Canny edge detection operator[40] applied to the T1ρ 20 ms image identified candidate points for a line growing search along the bone-cartilage interface (BCI). The user selected anterior and posterior points bounding the femoral terminal sulcus region on the sagittal image with all Canny filter detected edges overlain in red (Figure 2-A). The closest points on the Canny-derived line became endpoints between which detected bone-cartilage interface voxels were recorded by next voxel progression using a sliding logic matrix (SLM) technique that applied a 3 x 3 logic matrix around an image voxel of interest. If a voxel in the 3 x 3 neighborhood was detected as an edge by the Canny filter, and its position had not been previously recorded, it was added to the end of the line. The logic matrix traversed over each new end of the line until the target boundary point was reached.

Lack of curvature in the pixelated sulcus boundary impeded identification of the BCI in some images. Additional automated processing between the sulcus boundaries (red plus signs in Figure 2-B) constructed a list of single voxels and the midpoints of any contiguous horizontal regions, so that a piecewise cubic Hermite interpolating polynomial could be fit.[41] Inflections in the

TABLE 2
Knee Injury Diagnostic MRI Panel

MRI Sequence	Time mm:ss	Slice Thickness and Spacing mm – mm	In-Plane Resolution	Primary Purpose mm × mm
Axial Localizer	0:19	8.0 – 9.6	0.78 × 0.78	Planning
Sagittal–Coronal Localizer	0:21	8.0 – 12	0.49 × 0.49	Planning
Sagittal Proton Density	4:34	2.2 – 2.2	0.31 × 0.31	Ligaments / meniscus
Sagittal T2 Fat Saturated	4:00	2.2 – 2.2	0.44 × 0.44	Bone bruise / osteochondral fracture / effusion
Coronal T2 Fat Saturated	4:30	3.0 – 3.0	0.36 × 0.36	Bone bruise / osteochondral fracture / effusion
Coronal T1	4:19	3.1 – 3.3	0.44 × 0.44	Ligaments / meniscus
Axial T2 Fat Saturated	3:21	3.5 – 4.2	0.63 × 0.63	Bone bruise / osteochondral fracture / effusion
Optional Add-on T1rho 2-D	3:00	4	0.55 × 0.55	Sample Cartilage Composition

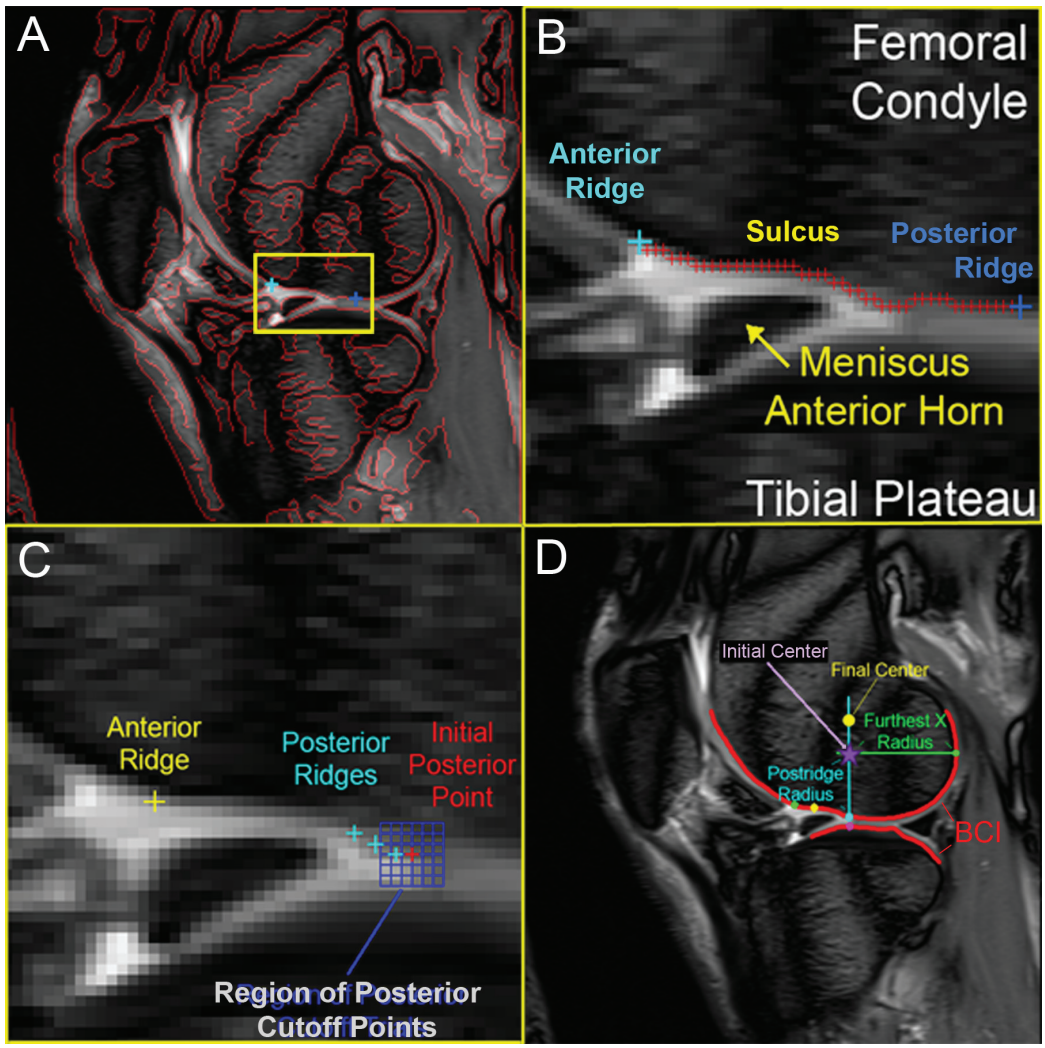

Figure 2. The direction-independent Canny filter identifies edges (red lines in A) on the 20ms T1ρ image. The user selects two points bounding the sulcus region (expanded in B) where geometric inflections objectively determine landmarks. The blue 7×7 grid test for objective posterior ridge location from likely user selected bounding points is added in C. The posterior condyle anthropometric reference center is located in panel D.

polynomial curve indicated geometric peaks and valleys in the knee's sulcus anatomy, thereby establishing the sulcus midpoint, anterior sulcus point, and posterior ridge point as anatomic landmarks. The anterior ridge was on the cusp between the anterior condyle and the rising slope of the sulcus; the sulcus midpoint was located at the peak of the sulcus dimple; and the posterior ridge point was on the cusp between the downward sulcus slope and the posterior condyle's curvature.

Variability of inter- and intra-user selection of anatomic landmarks was tested on three images that provided extremes in image clarity, definition of the variable geometry of the sulcus region, and typical sagittal slice geometries. After being briefly familiarized with general terms in the program, each of the three users was asked to pick the anterior and posterior cutoff points bounding the sulcus, four times for each image. Locations of these anatomic landmarks were recorded and compared for the 36 trials (3 images x 3 users x 4 trials). Sensitivity of the program to posterior cutoff point selection was further tested with a 7 x 7 grid (Figure 2-C). The user again selected two points bounding the sulcus region, and each posterior boundary's (x,y) coordinates were changed in single voxel increments, thereby examining 49 available voxels within a 3.8 x 3.8 mm^2 neighborhood as the potential posterior boundary site. The 49 adjusted posterior ridge locations were recorded to assess the program's objective correction for subjective user selection of sulcus bounds.

Once anatomic landmarks were identified, the SLM technique was applied along the posterior condyle's bone-cartilage interface from the posterior ridge point. An ellipse fit to the pixelated BCI line, using least-squares criterion, defined a smooth BCI arc near the calcified cartilage tidemark identified on histology (Figure 3). Biological variation in the size and shape of femoral condyles required anthropometric normalization to directly compare zone-dependent cartilage MRI relaxation times across patients' knees. A central reference point was placed directly above the posterior ridge site, at the height of the most posterior point on the lateral condyle (Figure 2-D). The average distance from this initial center to the posterior condyle and to the posterior ridge was defined as the anthropometric patient-specific femoral condyle radius, thereby placing the final center directly above the posterior ridge. This focal point approximated the posterior condyle's center of rotation, around which data were collected along the weight-bearing cartilage in a physiologically and biomechanically meaningful way.

The T1ρ relaxation times were sampled at 1° increments from the posterior ridge of the fitted bone-cartilage interface, and along 91 associated plane normals in 0.5 mm increments toward the cartilage surface, to create profiles approximating deep, radial and transitional cartilage zones. Each assigned T1ρ value resulted from the bilinear interpolation of the four nearest voxels. Inter-patient profile data along the 90° of knee flexion surface were combined into a normalized T1ρ database of zone-dependent weight-bearing articular cartilage.

In addition to the repeatability of anatomic landmark identification between scanning sessions and observers, the actual shapes of the bone-cartilage interface profiles were registered temporally across the Monday (Day 1), Wednesday (Day 3), and Friday (Day 5) scanning sessions for five normal knees, to verify anatomic coincidence. The posterior ridge point and a point 30 mm along the posterior condyle profile of each day's BCI line profile were identified. The line profiles for the latter two sessions were analytically translated and rotated to align with posterior ridge location on Day 1. The locations of each profile point were plotted directly on the common coordinate system from Day 1's image and the distances between corresponding points were analyzed.

Clinical application of whole-joint 3-dimensional T1ρ evaluation may require fewer image capture times. To assess the effects of reducing the number of spin-lock times on absolute T1ρ values, all permutations of 4 or more spin-lock times were used to create 990 new images from 15 normal subject MRI data sets (15 studies × 3 slices per study × 22 combinations per slice; 1 with 6 times, 6 with 5 times, 15 with 4 times). Selected maps were compared to results from reported 3-D sequence studies.[29, 42]

RESULTS

Osteochondral histology section 14 from the AKA knee (Figure 1) was imaged through a microscope's 4× objective lens and displayed with the scaled outline of a typical MRI slice (Figure 3).

Objective BCI location and T1ρ cartilage composition sampling

The three users' selections of sulcus bounding landmarks (Figure 2B) on three images were recorded and compared with the algorithm-derived locations of the posterior ridges for the 36 trials (Table 3).

Consistency of the objective posterior ridge point location was also tested systematically using an automated iterative process of a 7 x 7 grid in a 3.8 x 3.8mm square (Figure 2C). The algorithm reduced the 49 starting points to three locations of the posterior ridge on the Canny-derived bone-cartilage interface line. The preponderance of points (34) converged on one location; thirteen progressed to a point 1.5mm (3 voxels) closer to the sulcus, and two located 1 mm (2 voxels) farther

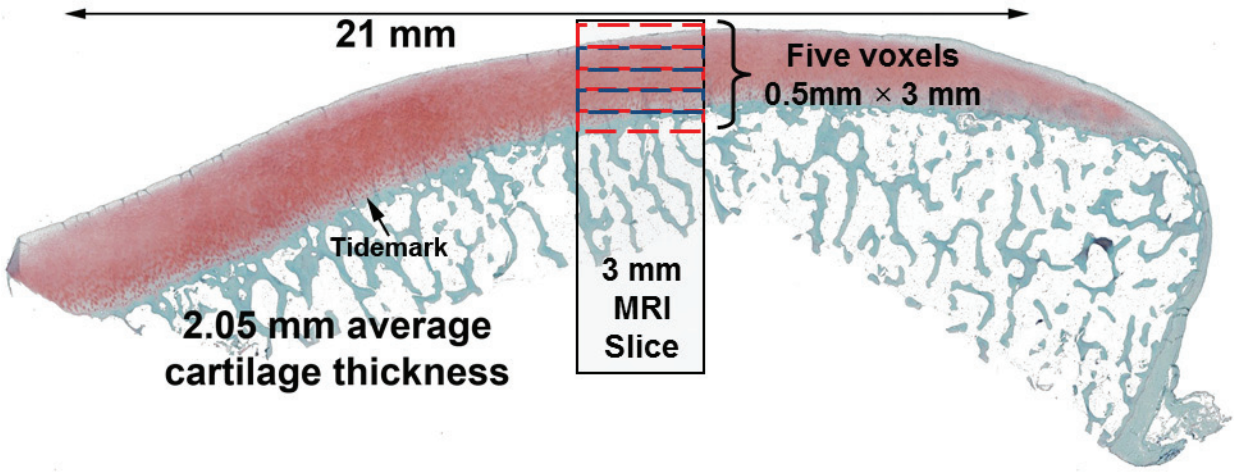

Figure 3. Coronal cartilage composition sampled by a 3mm thick MRI slice that has 0.5mm×0.5mm sagittal plane resolution. The 5 voxels sample the entire signal from the bone-cartilage interface (BCI), deep, radial, transitional and superficial cartilage zones. The BCI and superficial voxels illustrate volume-fraction sampling at the cartilage perimeter

Table 3

Distances (mm) between and number of unique landmark points found (12 possible for each point from 12 trials for each image). Average distances (standard deviation) and [maximum distance] are listed for each set of points in mm. AC=user-selected anterior cutoff points, PC=user-selected posterior cutoff points, PR=posterior ridge points after objective relocation to sulcus geometry. The combined maximum distances show the average of the maximum values (standard deviation) for the three images analyzed.

Normal Subject # (slice)	#of user AC	Distance Between AC	# of user PC	Distance Between PC	# of final PR	Distance Between PR
3 (lateral)	10	2.01 (± 1.27) [5.04]	7	0.96 (± 0.55) [2.25]	2	1.20 (± 1.13) [2.25]
4 (midline)	9	2.39 (± 2.18) [6.24]	4	0.75 (± 0.64)		
[2.25]	1	0.00 (± 0.00) [0.00]				
5 (lateral)	7	0.95 (± 0.66) [2.95]	6	0.75 (± 0.45) [1.73]	2	0.65 (± 0.62) [1.22
Combined Maximum Distance (std dev)		4.74 (±1.66)		2.08 (±0.30)		1.16 (±1.13)

down the sulcus wall. This demonstrated that for 49 potential user selections within a 7 x 7 neighborhood the program identified the same posterior ridge point 69.4% of the time.

The posterior ridge was selected as the anatomic reference point due to its clarity across subjects compared to the other landmark points (anterior ridge, sulcus midpoint). Anatomic coincidence of this common reference point in multi-day images was followed by image rotation to align the 30mm point along each posterior condyle (BCI profile in Figure 2D). The average distance between paired points was 0.289 mm ± 0.294 mm (approximately half the dimension of a voxel). The effect of MR technician alignment of oblique sagittal image planes on multiple days was evident in one outlier that showed curvature effects at the condyle edge increased average bone-cartilage interface point separation to approximately two voxels (1mm). In addition to anatomic coincidence, the range of T1ρ values from day1-to-day 3-to-day 5 for any given cartilage location was less than 10ms, demonstrating consistency of cartilage-composition sampling.

The establishment of an objective MR image co-registration with anthropometric normalization to the lateral femoral condyle enabled merging of data across knees to generate zone-dependent normal knee T1ρ relaxation values over the 90° weight-bearing region of the lateral condyle using the same six spin-lock times (Figure 4).

The AKA knee's lateral condyle midline histology sections are displayed with the enclosing T1ρ slice's

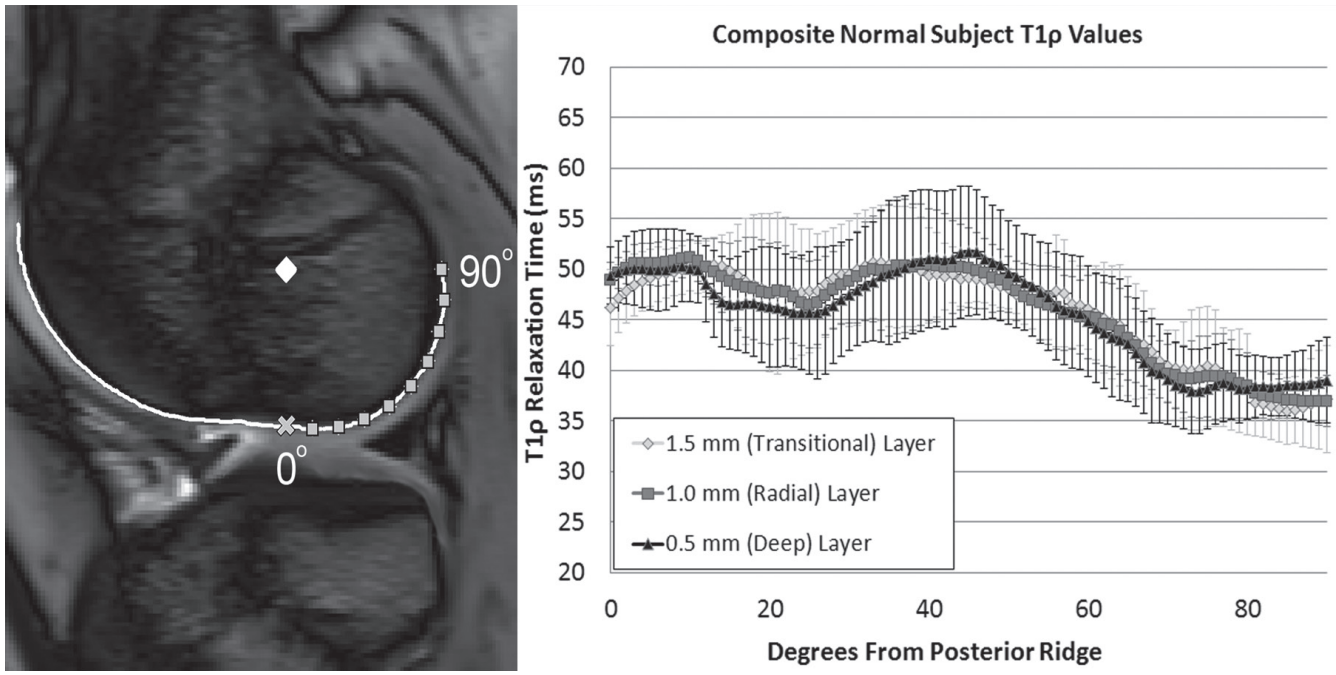

Figure 4. Normal zone-dependent T1ρ relaxation values (±1 standard deviation). The inset image shows the Normal Subject 4's bone-cartilage interface line, the anthropometric central reference point (diamond), and the posterior ridge (x). The squares indicate 10° increments along the bone-cartilage interface.

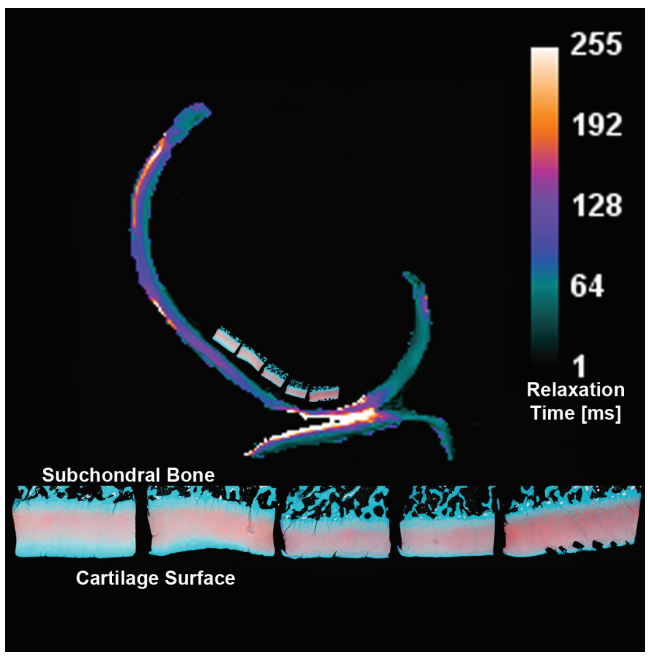

Figure 5. The AKA knee's mid-condylar T1ρ relaxation time contours are presented with the enclosed cartilage histology sections along the midline from face 15 to 11 in Figure 1.

relaxation times calculated for a reduced set of 12, 20, 40 and 60 ms spin-lock times (Figure 5). The effects of reduced spin-lock times are also shown in T1ρ maps for a single slice using six, five and four spin-lock times in the calculation of water proton relaxation times (Figure 6).

DISCUSSION

Direct comparison of cartilage-specific MRI relaxation parameters and changes in those values over time is enhanced by consistent, objective identification of a local anatomic feature. The target of this investigation was to create an objective method that could track the response of the lateral knee condyle to the blunt trauma of acute ACL rupture using line profiles through the articular cartilage. This isolated trauma and the articular cartilage response are believed to play a role in the early pathogenesis of post-traumatic osteoarthritis.[43, 44]

Using histology slice 14 as an example (Figure 3), the cartilage composition perpendicular to the MRI slice displays relatively uniform distribution of PG content across the weight-bearing region (red Safranin-O stain). The 5μm thick section and its next 99 neighbors together provided the signal for each cartilage-specific MRI voxel. Due to the consistent PG content in the region there is obvious latitude to slide the MRI slices right-or-left within the section(s) and return a similar set of relaxation times. Moreover, similar continuity is expected among sections cut through areas of the lateral femoral condyle damaged by impact during tibial subluxation in an acute ACL rupture.

Overall, user-selected anatomic landmark locations varied from 2.95 to 6.24 mm separation for the anterior sulcus boundary, and from 1.73 to 2.25 mm for posterior sulcus boundary points (Table 3). Computer algorithm results with objective geometric adjustment in the poste-

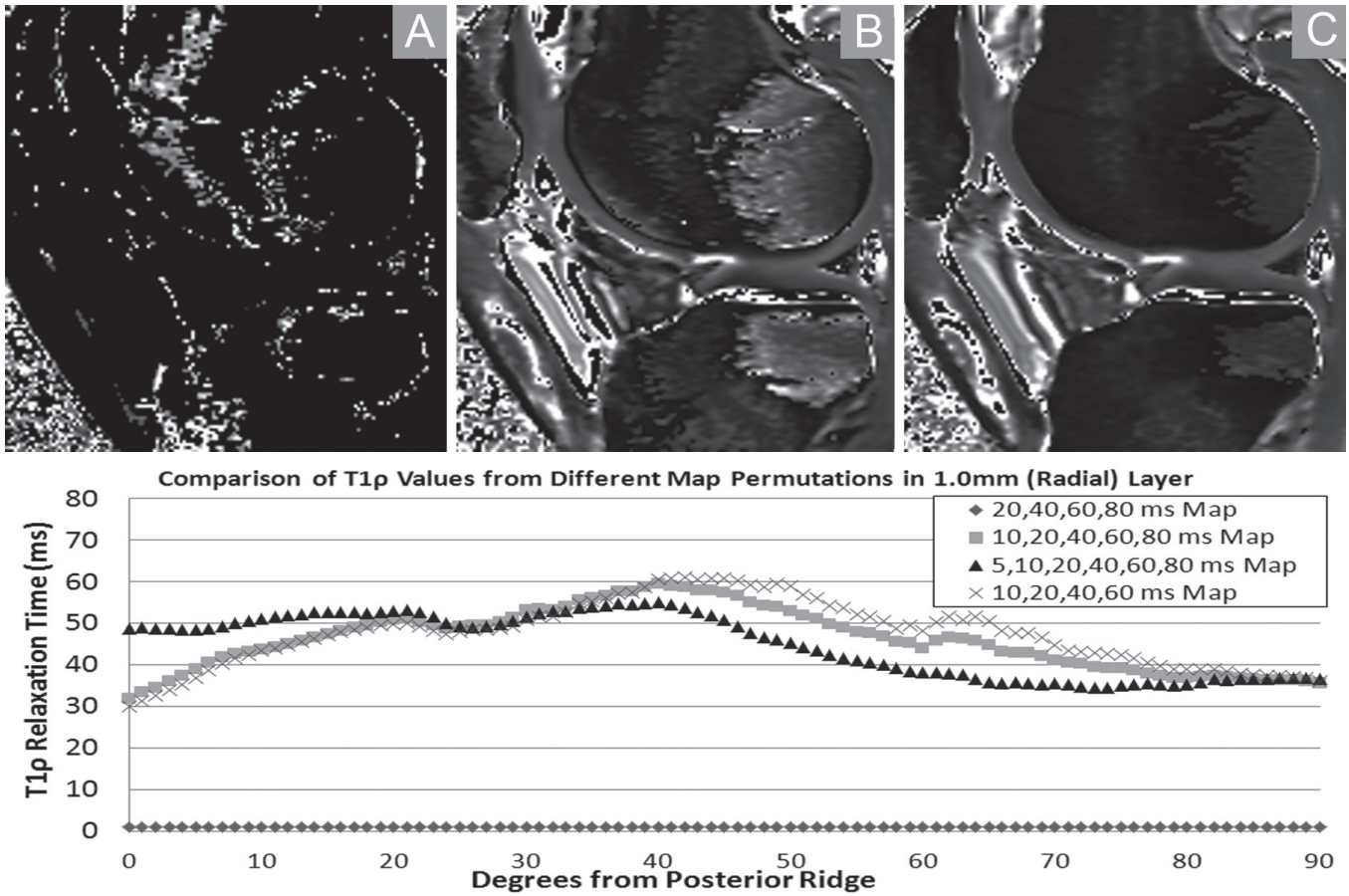

Figure 6. The effects of using different subsets of spin-lock times to calculate T1ρ relaxation times are demonstrated by comparing the translational cartilage zone evaluations for normal knee 4. Panel A used 20, 40, 60 and 80ms (diamond) values reported by Li et al.[1] Panel A times are most analogous to the AKA knee contours in Figure 6. Panel B shows the effect of adding the 10 ms spin-lock time to the T1ρ calculations (squares). The full set of six time points collected for the 2-D T1ρ evaluations in this study (Panel C) are denoted by the triangles.

rior ridge identification reduced variability by at least 50% from the user-selected sulcus boundary points. These results were formally verified by imposing a neighborhood grid and condensing 49 potential voxels to one site 70% of the time. The same site was identified as long as the user-selected point was not too near the sulcus.

Slice location imprecision from different scanning sessions is inherent within the setup of 2-D multi-slice MRI, potentially resulting in different geometries of the bone-cartilage interface and therefore different line profile curvatures. However, since our method yielded average differences in curvature geometry of much less than 0.5 mm (1 voxel) between corresponding points, in-plane differences should be minimal for this 2-D clinical application. Given the continuity of the underlying cartilage composition being assessed (Figure 2) and the dimensions of cartilage-specific T1ρ voxels sampling the PG-water proton interactions (Figure 3), 2-D T1ρ relaxation times through the midline of the lateral femoral condyle provide a step forward in noninvasive diagnostic assessment of cartilage condition. The composite normal T1ρ values within the weight-bearing cartilage of the posterior condyle demonstrated a consistently narrow envelope against which traumatic contusions of acute ACL rupture injuries may be quantified (Figure 4).

A limitation of this study was the incomplete MRI coverage of the knee. Because much of the initial damage occurs in the lateral compartment and subsequent PTOA observations and lesions often occur in the medial compartments, the initial focus was on early lateral knee articular cartilage response to injury. As 3-D methods of cartilage-composition imaging move from the necessary long scan-time constraints and complexities of research techniques for early injury diagnosis, they may well be combined with the needs of morphometric 3-D sequences used later in the OA disease progression to provide a more complete diagnostic and outcomes measure.

At this point in time, however, the reduced number of spin-lock times acquired to calculate T1ρ relaxation times for cartilage composition assessment requires more

validation and standardization. This is demonstrated by combining AKA lateral condyle mid-line histology with the T1ρ relaxation time profile generated for an MRI slice encompassing the sampled cartilage composition (Figure 5). The 12, 20, 40, 60 ms spin-lock time set did not produce T1ρ contours visually consistent with histologic staining. The sensitivity of reported T1ρ evaluations of articular cartilage was investigated using many permutations of spin-lock times to calculate the water proton-PG relaxation time constants. From a set of 6 spin-lock times used to generate the 2-D T1ρ evaluation in this study (Figure 6C), a subset using the 20, 40, 60, 80 ms subset reported by Li et al[5, 29, 45] (Figure 6A), and with an additional 10 ms time point (Figure 6B) are presented. Differences are visually apparent as well as quantifiably different. Add in the fact that different imaging hardware and different image capture protocols were used to acquire T1ρ relaxation times, it is apparent that direct comparisons of 3-D studies to 2-D evaluations of the underlying physical consistency of water proton interactions within the cartilage matrix require better standardization for clinical diagnostic applications.

For this study, relaxation times were recorded at set 0.5 mm increments outward from the bone-cartilage interface. This increment is consistent with attainable voxel size and it provides an observational path for retained cartilage based on the fact that erosion progresses downward from the surface. The method minimizes volume-fraction effects near the bone-cartilage-interface. Second, data sampled at normalized cartilage thickness levels would require segmentation of the superficial cartilage surface from surrounding tissue, which may be considered an elusive automation. And, in temporal series of post-traumatic osteoarthritis changes, thinning of the cartilage affects cartilage zonal definitions. By sampling at set intervals as here presented, the user is able to track changes at the same perpendicular locations over time.

CONCLUSIONS

A lateral condyle-specific registration method has been developed for T1ρ MRI, a sequence with demonstrated sensitivity to cartilage composition changes during recovery from acute ACL trauma. Validation tests of this method confirm bone-cartilage interface registration reliability, and multiple-day imaging of normal knees demonstrates consistency of zone-dependent T1ρ imaging of cartilage, even with variability in patient-specific posterior ridge geometry. The developed image analysis tools serve as the first step toward quantitative functional assessment of cartilage health with noninvasive T1ρ MRI, which has the potential to become an important new tool for the early diagnosis of cartilage degeneration following ACL trauma.

ACKNOWLEDGEMENTS

Funding provided by NIH NIAMS P50 AR055533 and AOSSM Research Grant.

REFERENCES

1. **Cheng YJ, Hootman JM, Murphy LB, Langmaid GA, Helmick CG.** Prevalence of doctor-diagnosed arthritis and arthritis-attributable activity limitation - united states, 2007-2009. In: *HHS*, editor.: Centers for Disease Control and Prevention; 2010. p. 1261-5.
2. **Buckwalter JA, Saltzman C, Brown T.** The impact of osteoarthritis: Implications for research. *Clinical orthopaedics and related research.* 2004(427 Suppl):S6-15.
3. **Gold GE, Thedens DR, Pauly JM, Fechner KP, Bergman G, Beaulieu CF, et al.** Mr imaging of articular cartilage of the knee: New methods using ultrashort tes. *AJR Am J Roentgenol.* 1998;170(5):1223-6.
4. Osteoarthritis initiative: Oai [database on the Internet]. www.oai.ucsf.edu. 2006.
5. **Carballido-Gamio J, Bauer JS, Stahl R, Lee KY, Krause S, Link TM, et al.** Inter-subject comparison of mri knee cartilage thickness. *Medical image analysis.* 2008;12(2):120-35.
6. **Hohe J, Faber S, Muehlbauer R, Reiser M, Englmeier KH, Eckstein F.** Three-dimensional analysis and visualization of regional mr signal intensity distribution of articular cartilage. *Medical engineering & physics.* 2002;24(3):219-27.
7. **Lerner AL, Tamez-Pena JG, Houck JR, Yao J, Harmon HL, Salo AD, et al.** The use of sequential mr image sets for determining tibiofemoral motion: Reliability of coordinate systems and accuracy of motion tracking algorithm. *Journal of biomechanical engineering.* 2003;125(2):246-53.
8. **Williams TG, Holmes AP, Waterton JC, Maciewicz RA, Hutchinson CE, Moots RJ, et al.** Anatomically corresponded regional analysis of cartilage in asymptomatic and osteoarthritic knees by statistical shape modelling of the bone. *IEEE transactions on medical imaging.* 29(8):1541-59.
9. **Eckstein F, Ateshian G, Burgkart R, Burstein D, Cicuttini F, Dardzinski B, et al.** Proposal for a nomenclature for magnetic resonance imaging based measures of articular cartilage in osteoarthritis. *Osteoarthritis and cartilage / OARS,* Osteoarthritis Research Society. 2006;14(10):974-83.
10. **Peterfy CG, Guermazi A, Zaim S, Tirman PF, Miaux Y, White D, et al.** Whole-organ magnetic resonance imaging score (worms) of the knee in osteoarthritis. *Osteoarthritis and cartilage / OARS,* Osteoarthritis Research Society. 2004;12(3):177-90.

11. **Eckstein F, Yang M, Guermazi A, Roemer FW, Hudelmaier M, Picha K, et al.** Reference values and z-scores for subregional femorotibial cartilage thickness - results from a large population-based sample (framingham) and comparison with the non-exposed osteoarthritis initiative reference cohort. *Osteoarthritis and cartilage / OARS*, Osteoarthritis Research Society.
12. **Frobell RB, Wirth W, Nevitt M, Wyman BT, Benichou O, Dreher D, et al.** Presence, location, type and size of denuded areas of subchondral bone in the knee as a function of radiographic stage of oa - data from the oa initiative. *Osteoarthritis and cartilage / OARS*, Osteoarthritis Research Society.18(5):668-76.
13. **Buckwalter JA, Brown TD.** Joint injury, repair, and remodeling: Roles in post-traumatic osteoarthritis. *Clinical orthopaedics and related research.* 2004(423):7-16.
14. **Blumenkrantz G, Majumdar S.** Quantitative magnetic resonance imaging of articular cartilage in osteoarthritis. *European cells & materials.* 2007;13:76-86.
15. **Bruno MA, Mosher TJ, Gold GE.** *Arthritis in color: Advanced imaging of arthritis.* 1 ed: Saunders Elsevier; 2009.
16. **Thedens DR, Martin JA, Pedersen DR.** Magnetic resonance imaging of cartilage: New imaging and clinical approaches. In: Buckwalter JA, Lotz M, Stoltz J-F, editors. *Osteoarthritis, inflammation and degradation: A continuum.* Amsterdam: IOS Press; 2007. p. 239-53.
17. **Liess C, Lusse S, Karger N, Heller M, Gluer CC.** Detection of changes in cartilage water content using mri t2-mapping in vivo. *Osteoarthritis and cartilage / OARS*, Osteoarthritis Research Society. 2002;10(12):907-13.
18. **Nieminen MT, Rieppo J, Toyras J, Hakumaki JM, Silvennoinen J, Hyttinen MM, et al.** T2 relaxation reveals spatial collagen architecture in articular cartilage: A comparative quantitative mri and polarized light microscopic study. *Magn Reson Med.* 2001;46(3):487-93.
19. **Raya JG, Horng A, Dietrich O, Weber J, Dinges J, Mutzel E, et al.** Voxel-based reproducibility of t2 relaxation time in patellar cartilage at 1.5 t with a new validated 3d rigid registration algorithm. *Magma* (New York, NY. 2009;22(4):229-39.
20. **Xia Y, Moody JB, Alhadlaq H.** Orientational dependence of t2 relaxation in articular cartilage: A microscopic mri (micromri) study. *Magn Reson Med.* 2002;48(3):460-9.
21. **Bashir A, Gray ML, Hartke J, Burstein D.** Nondestructive imaging of human cartilage glycosaminoglycan concentration by mri. *Magn Reson Med.* 1999;41(5):857-65.
22. **Gray ML, Burstein D, Kim YJ, Maroudas A.** 2007 elizabeth winston lanier award winner. Magnetic resonance imaging of cartilage glycosaminoglycan: Basic principles, imaging technique, and clinical applications. *J Orthop Res.* 2008;26(3):281-91.
23. **Gray ML, Eckstein F, Peterfy C, Dahlberg L, Kim YJ, Sorensen AG.** Toward imaging biomarkers for osteoarthritis. *Clinical orthopaedics and related research.* 2004(427 Suppl):S175-81.
24. **Broome DR, Girguis MS, Baron PW, Cottrell AC, Kjellin I, Kirk GA.** Gadodiamide-associated nephrogenic systemic fibrosis: Why radiologists should be concerned. *AJR Am J Roentgenol.* 2007;188(2):586-92.
25. **Sadowski EA, Bennett LK, Chan MR, Wentland AL, Garrett AL, Garrett RW, et al.** Nephrogenic systemic fibrosis: Risk factors and incidence estimation. *Radiology.* 2007;243(1):148-57.
26. **Duvvuri U, Goldberg AD, Kranz JK, Hoang L, Reddy R, Wehrli FW, et al.** Water magnetic relaxation dispersion in biological systems: The contribution of proton exchange and implications for the noninvasive detection of cartilage degradation. *Proceedings of the National Academy of Sciences of the United States of America.* 2001;98(22):12479-84.
27. **Duvvuri U, Kudchodkar S, Reddy R, Leigh JS.** T(1rho) relaxation can assess longitudinal proteoglycan loss from articular cartilage in vitro. *Osteoarthritis and cartilage / OARS*, Osteoarthritis Research Society. 2002;10(11):838-44.
28. **Wheaton AJ, Dodge GR, Elliott DM, Nicoll SB, Reddy R.** Quantification of cartilage biomechanical and biochemical properties via t1rho magnetic resonance imaging. *Magn Reson Med.* 2005;54(5):1087-93.
29. **Li X, Kuo D, Theologis A, Carballido-Gamio J, Stehling C, Link TM, et al.** Cartilage in anterior cruciate ligament-reconstructed knees: Mr imaging t1{rho} and t2–initial experience with 1-year follow-up. *Radiology.* 258(2):505-14.
30. **Peterfy CG, Gold G, Eckstein F, Cicuttini F, Dardzinski B, Stevens R.** Mri protocols for whole-organ assessment of the knee in osteoarthritis. *Osteoarthritis and cartilage / OARS*, Osteoarthritis Research Society. 2006;14 Suppl A:A95-111.
31. **Vellet AD, Marks P, Fowler P, Munro T.** Accuracy of nonorthogonal magnetic resonance imaging in acute disruption of the anterior cruciate ligament. *Arthroscopy.* 1989;5(4):287-93.

32. **Hunziker EB.** Articular cartilage repair: Basic science and clinical progress. A review of the current status and prospects. *Osteoarthritis and cartilage / OARS*, Osteoarthritis Research Society. 2002;10(6):432-63.
33. **Mainil-Varlet P, Van Damme B, Nesic D, Knutsen G, Kandel R, Roberts S.** A new histology scoring system for the assessment of the quality of human cartilage repair: Icrs ii. *The American journal of sports medicine.* 38(5):880-90.
34. **O'Driscoll SW, Marx RG, Beaton DE, Miura Y, Gallay SH, Fitzsimmons JS.** Validation of a simple histological-histochemical cartilage scoring system. *Tissue engineering.* 2001;7(3):313-20.
35. **Pritzker KP, Gay S, Jimenez SA, Ostergaard K, Pelletier JP, Revell PA, et al.** Osteoarthritis cartilage histopathology: Grading and staging. *Osteoarthritis and cartilage / OARS*, Osteoarthritis Research Society. 2006;14(1):13-29.
36. **Mankin HJ, Dorfman H, Lippiello L, Zarins A.** Biochemical and metabolic abnormalities in articular cartilage from osteo-arthritic human hips. Ii. Correlation of morphology with biochemical and metabolic data. *J Bone Joint Surg Am.* 1971;53(3):523-37.
37. **Moussavi-Harami SF, Pedersen DR, Martin JA, Hillis SL, Brown TD**. Automated objective scoring of histologically apparent cartilage degeneration using a custom image analysis program. *J Orthop Res.* 2009;27(4):522-8.
38. **Rosenberg L.** Chemical basis for the histological use of safranin o in the study of articular cartilage. *J Bone Joint Surg Am.* 1971;53(1):69-82.
39. **Charagundla SR, Borthakur A, Leigh JS, Reddy R.** Artifacts in t(1rho)-weighted imaging: Correction with a self-compensating spin-locking pulse. *J Magn Reson.* 2003;162(1):113-21.
40. **Canny J.** A computational approach to edge detection. Pattern Analysis and Machine Intelligence, *IEEE Transactions on.* 1986; PAMI-8(6):679-98.
41. **Fritsch FN, Carlson RE.** Monotone piecewise cubic interpolation. *SIAM Journal on Numerical Analysis.* 1980;17(2):238-46.
42. **Keenan KE, Besier TF, Pauly JM, Han E, Rosenberg J, Smith RL, et al.** Prediction of glycosaminoglycan content in human cartilage by age, t1rho and t2 mri. *Osteoarthritis and cartilage / OARS*, Osteoarthritis Research Society. 19(2):171-9.
43. **Hunter D, Li J, LaValley M, Bauer D, Nevitt M, DeGroot J, et al.** Cartilage markers and their association with cartilage loss on magnetic resonance imaging in knee osteoarthritis: The boston osteoarthritis knee study. *Arthritis Research & Therapy.* 2007;9(5):R108.
44. **Lohmander LS, Englund PM, Dahl LL, Roos EM.** The long-term consequence of anterior cruciate ligament and meniscus injuries. *The American journal of sports medicine.* 2007;35(10):1756-69.
45. **Stahl R, Luke A, Li X, Carballido-Gamio J, Ma CB, Majumdar S, et al.** T1rho, t2 and focal knee cartilage abnormalities in physically active and sedentary healthy subjects versus early oa patients--a 3.0-tesla mri study. *European radiology.* 2009;19(1):132-43.